www.lajss.org
Latin American Journal of Solids and Structures 2 (2005) 65–76

Finite elements with embedded multiple cracks and non-uniform discontinuity modes

O. L. Manzoli[a,*] and P. B. Shing[b]

[a]Department of Civil Engineering, State of Sao Paulo University, Bauru, SP 17033-360, Brazil
[a]Department of Structural Engineering, University of California at San Diego, La Jolla, CA 92093, USA

Abstract

Recently, several formulations of finite elements embedded with displacement discontinuity have been proposed to describe crack propagation independent of the element boundaries. By construction, these approaches are limited to represent a single crack in the element with uniform discontinuity modes (opening and sliding). This paper presents a procedure to embed displacement discontinuities in quadrilateral finite elements that is suitable for incorporating multiple discontinuities or non-uniform discontinuity modes. These capabilities may be essential to predict failure in reinforced concrete. Basic tests are performed to access the effectiveness of the proposed technique

1 Introduction

In the last years the embedded discontinuity elements has been showed to be a valuable technique for numerical prediction in failure mechanics. This technique is based on the enrichment of the kinematic fields of the finite element to represent an internal displacement discontinuity interface independent of the element boundaries. The main benefit of this class of approach is that the propagation of the discontinuity can be captured using a fixed finite element mesh defined prior to the analysis, even when the discontinuity path is not known in advance. A comparative study of several embedded discontinuity element formulations proposed has been performed by Jirásek [3]. As shown in this study, only the non-symmetric approaches [1, 4, 6], classified as statically and kinematically optimal non-symmetric (SKON), are able to properly represent the kinematics of the discontinuity as well as the relationship between the stress in the bulk of the element and the tractions across the discontinuity interface.

* Corresponding author E-mail: omanzoli@feb.unesp.br
Received 19 November 2004
From *Recent Developments in the Modelling of Rupture in Solids Conference*, ed. A. Benallal & S.P.B. Proença.

Notation

Ω_e	Finite element domain
S	Discontinuity interface
$(\bar{x},\bar{y})$	Interface coordinate system
$\mathbf{n}$	Unit vector normal to S
$\mathbf{u}$	Total displacement field
$\tilde{\mathbf{u}}$	Displacement field of the continuum portion
$\hat{\mathbf{u}}$	Displacement field related to the relative rigid-body motion due to the discontinuity
$\mathbf{u}_h, \hat{\mathbf{u}}_h, \tilde{\mathbf{u}}_h$	Displacement vectors
$H(\bar{x})$	Heaviside function defined in Ω_e ($H(\bar{x}) = 1$if $\bar{x} > 0$ and $H(\bar{x}) = 0$ otherwise)
$[[\mathbf{u}]]$	Vector containing the components of the displacement jump
$\mathbf{d}$	Nodal displacement vector
$\hat{\mathbf{d}}$	Vector containing the nodal displacement due to the relative rigid-body motion
P	Projection matrix
$\boldsymbol{\varepsilon}_h, \hat{\boldsymbol{\varepsilon}}_h, \tilde{\boldsymbol{\varepsilon}}_h$	Strain vectors
$\tilde{\boldsymbol{\sigma}}_h$	Stress vector of the continuum
$\mathbf{N}$, B	Standard finite element conforming shape function matrix and strain-displacement matrix
E	Elastic material matrix
A	Finite element assembly operator
$\mathbf{f}_{int_e}, \mathbf{f}_{ext_e}$	Vectors of internal and external nodal forces
$\tilde{\mathbf{K}}_e$	Standard elastic finite element stiffness matrix
$\mathbf{t}_S$	Traction vector in the interface
$\Sigma^d(\bullet)$	Discrete constitutive law
$\Sigma^c(\bullet)$	Continuum-type constitutive law
$\mathbf{N_n}$	Matrix that extracts the traction vector related to a surface with unit normal vector $\mathbf{n}$ from the stress vector
δ_S	Dirac delta distribution placed in S
k	Delta regularization parameter
Q	Collocation point at the discontinuity interface.
l	Distance between two collocation points in S
$\mathbf{K}_e$	Condensed stiffness matrix
$\boldsymbol{\varepsilon}^p, \lambda$	Plastic strain vector and plastic multiplier
q	Hardening/softening internal variable
H	Hardening/softening modulus
ϕ	Yield function
$\bar{H}$	Intrinsic or discrete softening modulus
$\mathbf{S}$, p	Deviatoric stress and mean stress
f_t, G_F	Tensile strength and fracture energy
E, υ	Young's modulus and Poisson's ratio

In despite of the good potential of the SKON approaches, its application in fracture mechanics has been limited to represent a single crack in the element with uniform discontinuity modes. This intrinsic

limitation of the SKON approach is a consequence of the average form to enforce traction continuity inside and outside the crack line, taking no advantage of higher-order terms in the stress field of quadrilateral elements. The multiple-discontinuity capability is desirable when several discontinuities are expected in small regions (e.g., crack formation in reinforced concrete) or when non-proportional loads can induce new discontinuities intercepting old ones. As it is shown in this paper, the non-uniform modes can be essential to avoid stress locking in quadrilateral finite elements subjected to bending-type deformation.

This paper presents a procedure to embed discontinuities in quadrilateral elements that is more suitable for incorporating multiple discontinuities or non-uniform discontinuity modes. The procedure distinguishes the kinematic fields associated to the deformation of the solid portion of the element from the one related to the rigid-body motion due to the internal displacement discontinuity. The finite element equations for the original underlying elements (without discontinuity) are used to represent the solid portion. A constitutive relation between the relative displacements and tractions describes the discontinuity interface. This constitutive relation can be given directly by a discrete interface constitutive law or it can result from a continuum-type (stress-strain) constitutive law, according to the regularized strong discontinuity approach [5,7]. Imposing traction continuity condition at collocation points located in the discontinuity interface enforces the coupling between the solid portion and the discontinuity interface.

Numerical tests are carried out to access the performance of the proposed technique for quadrilateral elements with embedded displacement discontinuities.

2 Embedded discontinuity element

2.1 Decomposition of the displacement field

Consider the finite element domain $\Omega_e$that is divided by the discontinuity interface S into regions Ω_e^+ and Ω_e^- as showed in Figure 1a. Consider also the interface coordinate system $(\bar{x},\bar{y})$, such that $\bar{x}$ is normal to the discontinuity interface pointing towards Ω_e^+.

The displacement field, $\mathbf{u}$, inside the element can be decomposed into a component associated with the deformation of the continuum portion, $\tilde{\mathbf{u}}$, and a component related to the rigid-body relative motion, $\hat{\mathbf{u}}$, between the two parts of the element (see Figure 1b):

$$\mathbf{u} = \tilde{\mathbf{u}} + \hat{\mathbf{u}} \tag{1}$$

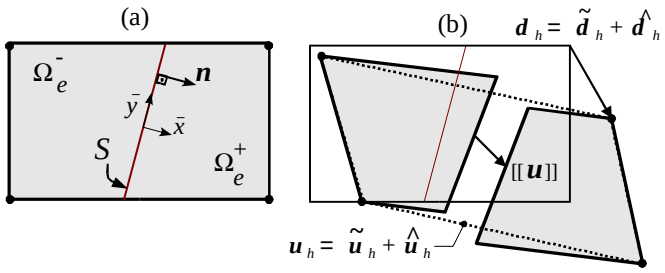

Figure 1: Decomposition of the displacement field.

If the relative interface motion is assumed uniform in the element, the relative rigid-body part can be expressed as

$$\hat{\mathbf{u}} = H(\bar{x})\,[[\mathbf{u}]] \tag{2}$$

2.2 Finite element approximation

The continuous approximation of the displacement field can be obtained using the standard finite element conforming shape function matrix $\mathbf{N}$ as:

$$\mathbf{u}_h = \mathbf{N}\,\mathbf{d} \tag{3}$$

so that

$$\boldsymbol{\varepsilon}_h = \mathbf{B}\,\mathbf{d} \tag{4}$$

The continuous approximation of the relative rigid-body component can be expressed as:

$$\hat{\mathbf{u}}_h = \mathbf{N}\,\hat{\mathbf{d}} \tag{5}$$

If the relative interface motion is assumed uniform in the element, $\hat{\mathbf{d}}$ is given by

$$\hat{\mathbf{d}} = \mathbf{P}\;[[\mathbf{u}]] \tag{6}$$

with

$$\mathbf{P} = \begin{bmatrix} H(\bar{x}_1) & 0 \\ 0 & H(\bar{x}_1) \\ \vdots & \vdots \\ H(\bar{x}_{n_{ed}}) & \\ & H(\bar{x}_{n_{ed}}) \end{bmatrix} \tag{7}$$

where n_{ed} is the number of element nodes and $\bar{x}_i$ (i=1,2, n_{ed}) are the nodal coordinates.

The corresponding strain is given by

$$\hat{\boldsymbol{\varepsilon}}_h = \mathbf{B}\,\hat{\mathbf{d}} = \mathbf{B}\,\mathbf{P}\;[[\mathbf{u}]] \tag{8}$$

Taking into account Eq.(1), Eq.(4) and Eq.(8), the strain field of the continuum portion is given by:

$$\tilde{\boldsymbol{\varepsilon}}_h = \boldsymbol{\varepsilon}_h - \hat{\boldsymbol{\varepsilon}}_h = \mathbf{B}\,(\mathbf{d} - \mathbf{P}\;[[\mathbf{u}]]) \tag{9}$$

For the sake of simplicity, the continuum is considered linearly elastic and isotropic. In this case, the corresponding stress field is obtained from the strain field Eq.(9) leading to the follow constitutive equation:

$$\tilde{\boldsymbol{\sigma}}_h = \mathbf{E}\,\tilde{\boldsymbol{\varepsilon}}_h \tag{10}$$

$$\tilde{\boldsymbol{\sigma}}_h = \mathbf{E}\,(\boldsymbol{\varepsilon}_h - \hat{\boldsymbol{\varepsilon}}_h) \tag{11}$$

$$\tilde{\boldsymbol{\sigma}}_h = \mathbf{E}\,\mathbf{B}\,(\mathbf{d} - \mathbf{P}\;[[\mathbf{u}]]) \tag{12}$$

The continuous approximation of the rigid-body motion, $\hat{\boldsymbol{\varepsilon}}_h$, can, then, be interpreted as an *equivalent continuous inelastic strain*, which releases stress in the continuum.

2.3 Finite element equations

Since the rigid-body component of the strain can be considered as an equivalent inelastic strain, the finite element equations of the underlying element can be used to describe the continuum portion:

$$\int_{\Omega} \mathbf{B}^T \, \tilde{\boldsymbol{\sigma}}_h \, d\Omega \, = \, \int_{\Omega} \mathbf{N}^T \, \bar{\mathbf{b}} \, d\Omega \, + \, \int_{\Gamma_t} \mathbf{N}^T \, \bar{\mathbf{t}} \, d\Gamma \tag{13}$$

where Ω is the domain of the body, Γ_t is the part of the boundary subjected to prescribed traction, $\bar{\mathbf{t}}$, and $\bar{\mathbf{b}}$ is the prescribed body forces. By taking into account the finite element approximations given by Eq.(11), Eq.(4) and Eq.(8), the Eq.(13) can be rewritten as

$$\overset{n_{el}}{\underset{e=1}{\mathrm{A}}} \, \mathbf{f}_{int_e} - \overset{n_{el}}{\underset{e=1}{\mathrm{A}}} \, \mathbf{f}_{ext_e} = \mathbf{0} \tag{14}$$

where

$$\mathbf{f}_{int_e} = \tilde{\mathbf{K}}_e(\mathbf{d} - \mathbf{P} \, [[\mathbf{u}]] \,) \tag{15}$$

$$\mathbf{f}_{ext_e} \, = \, \int_{\Omega_e} \mathbf{N}^T \, \bar{\mathbf{b}} \, d\Omega \, + \, \int_{\Gamma_{e_t}} \mathbf{N}^T \, \bar{\mathbf{t}} \, d\Gamma \tag{16}$$

in which

$$\tilde{\mathbf{K}}_e \, = \, \int_{\Omega_e} \mathbf{B}^T \mathbf{E} \, \mathbf{B} \, d\Omega \tag{17}$$

2.4 Non-linear behavior of the discontinuity interface

The non-linear behavior of the discontinuity interface can be described by means of a constitutive relation between the cohesive traction in the interface, $\mathbf{t}_S$, and the components of the displacement jump, $[[\mathbf{u}]]$. In non-linear fracture mechanics, this constitutive relation is given by an *adhoc* discrete law of the form:

$$\mathbf{t}_S = \Sigma^d(\, [[\mathbf{u}]]) \tag{18}$$

where $\Sigma^d(\bullet)$ gives the traction as a function of the jump and its history .

On the other hand, in the so-called strong discontinuity approach [5] the behavior of the interface is described by a continuum (stress vs. strain) non-linear constitutive law. A discrete constitutive law is induced by degenerating the continuum in a consistent manner. In this case, the traction vector in the interface is given by:

$$\mathbf{t}_S = \mathbf{N}_\mathbf{n} \, \Sigma^c(\, \varepsilon) \text{ in } S \tag{19}$$

where $\Sigma^c(\bullet)$ returns the stress from a given strain and its history. For two-dimensional problems, $N_\mathbf{n}$ is expressed as:

$$\mathbf{N}_\mathbf{n} \, = \, \begin{bmatrix} n_x & 0 & n_y \\ 0 & n_y & n_x \end{bmatrix} \tag{20}$$

where n_x and n_y are the components of $\mathbf{n}$.

The total strain field is obtained from the discontinuous displacement field, which can be recovered as follows:

$$\mathbf{u} = \tilde{\mathbf{u}}_h + \hat{\mathbf{u}} = \tilde{\mathbf{u}}_h \, + H(\bar{x}) \, [[\mathbf{u}]] \tag{21}$$

Taking the gradient of Eq.(21) leads to the corresponding strain field:

$$\boldsymbol{\varepsilon} = \tilde{\boldsymbol{\varepsilon}} + \delta_S \, \mathbf{N_n}^T \, [[\mathbf{u}]] \tag{22}$$

The last term of Eq.(22) introduces an unbounded component in the total strain field.
Thus, taking into account Eq.(22) and Eq.(9), Eq.(19) becomes:

$$\mathbf{t}_S = \mathbf{N_n} \Sigma^c \left(\mathbf{B}(\mathbf{d} - \mathbf{P} \, [[\mathbf{u}]]) + \frac{1}{k} \mathbf{N_n}^T \, [[\mathbf{u}]] \right) \tag{23}$$

For computational purposes, in Eq.(23), δ_S has been replaced by the approximation [6]:

$$\delta_S(\mathbf{x}) \approx \begin{cases} \frac{1}{k} & if \; \mathbf{x} \in S, \\ 0 & \text{otherwise.} \end{cases} \tag{24}$$

so that, when k tends to zero the approximation in (24) transforms into an exact Dirac delta distribution.

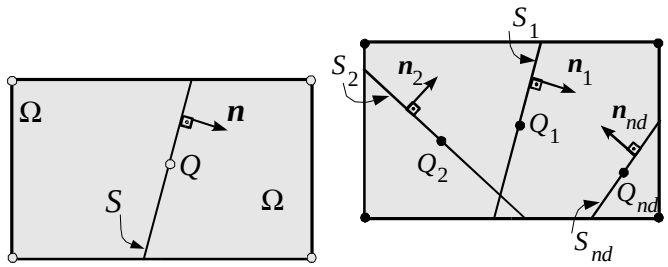

(a) (b)

Figure 2: Collocation points: (a) single interface, (b) multiple interfaces.

2.5 Coupling continuum and interface

The continuum and the interface can be coupled by means of the following condition:

$$\mathbf{t}_S - \mathbf{N_n} \, \boldsymbol{\sigma}_h = \mathbf{0} \quad \text{in } Q \in S \tag{25}$$

which enforces the traction continuity locally at the collocation point Q of the discontinuity interface (see figure 2a).

Taking into account the constitutive relation for the continuum Eq.(11) and the finite element approximation Eq.(9), the equilibrium equations Eq.(25) become:

$$\mathbf{t}_S(\mathbf{d}, \, [[\mathbf{u}]]) - \hat{\mathbf{K}}_e(\mathbf{d} - \mathbf{P} \, [[\mathbf{u}]]) = \mathbf{0} \;\; \text{at } Q \in S \tag{26}$$

where

$$\hat{\mathbf{K}}_e = \mathbf{N_n} \mathbf{E} \, \mathbf{B} \tag{27}$$

and the expression of $\mathbf{t}_S(\mathbf{d}, \, [[\mathbf{u}]])$ is given by Eq.(18) for the discrete interface approach or by Eq.(23) for the regularized strong discontinuity approach.

3 Multiple discontinuities

If more than one discontinuity interface is present in the element (see Figure 2b), the resulting rigid-body motion is the sum of those related to each interface:

$$\hat{\mathbf{u}} = \sum_{k=1}^{nd} H_k \left[[\mathbf{u}]\right]_k \tag{28}$$

where nd is the number of discontinuity interfaces in the element. H_k and $\left[[\mathbf{u}]\right]_k$ are the Heaviside function and the discontinuity modes of the kth discontinuity interface, S_k.

The corresponding nodal displacement vector is given by:

$$\hat{\mathbf{d}} = [\mathbf{P}] \; \{ \, [[\mathbf{u}]] \, \} \tag{29}$$

where the multiple-discontinuity matrix, $[\mathbf{P}]$, and vector, $\{ \, [[\mathbf{u}]] \, \}$, collect, respectively, the $\mathbf{P}$ matrices and $[[\mathbf{u}]]$ vectors for the individual interfaces.

The traction continuity Eq.(26) must be written for a collocation point in each interface of the element (see Figure 2b), yielding the following set of equations:

$$\{\mathbf{t}_S(\mathbf{d}, \, [[\mathbf{u}]])\} - [\hat{\mathbf{K}}_e] \, (\mathbf{d} - [\mathbf{P}] \; \{ \, [[\mathbf{u}]] \, \}) = \mathbf{0} \tag{30}$$

where

$$\{\mathbf{t}_S\} = \{ \; \mathbf{t}_{S_1} \quad \mathbf{t}_{S_2} \quad \ldots \quad \mathbf{t}_{S_{nd}} \; \}^T \tag{31}$$

$$[\hat{\mathbf{K}}_e] = \left[\; \hat{\mathbf{K}}_1 \quad \hat{\mathbf{K}}_2 \quad \ldots \quad \hat{\mathbf{K}}_{nd} \; \right]^T \tag{32}$$

grouping, respectively, the traction vectors, $\mathbf{t}_{S_k}$, and the $\hat{\mathbf{K}}_k$ matrices for each collocation point Q_k ($k = 1, \, nd$).

4 Solution scheme

In a non-linear displacement-based finite element analysis, the equilibrium equations are solved by means of an incremental-iterative scheme in which equality Eq.(14) is checked at each iteration for a given improved approximation of the nodal displacements. Thus, the element internal force vector and the tangent stiffness matrix have to be formed in each iteration.

For the embedded multiple discontinuities formulation, the equilibrium equations in the element level are given by Eq.(15) and Eq.(30), relating the variables of an element at the ith iteration of the nth loading step:

$$\mathbf{f}_{int_e}^{n,i} = \tilde{\mathbf{K}}_e(\mathbf{d}^{n,i} - [\mathbf{P}] \, \{ \, [[\mathbf{u}]] \, \}^{n,i}) \tag{33}$$

$$\left\{ \, \mathbf{t}_S(\mathbf{d}^{n,i}, \{ \, [[\mathbf{u}]] \, \}^{n,i}) \, \right\} = \left[\hat{\mathbf{K}}_e \right] \; (\mathbf{d}^{n,i} - [\mathbf{P}] \, \{ \, [[\mathbf{u}]] \, \}^{n,i}) \tag{34}$$

For a given $\mathbf{d}^{n,i}$, the extended system of non-linear Eq.(34) can be solved for $\{ \, [[\mathbf{u}]] \, \}^{n,i}$and the element internal forces vector can be evaluated directly by Eq.(33). The rate form of Eq.(33) and Eq.(34) can be cast into the following matrix form:

$$\begin{bmatrix} \mathbf{K}_e^{dd} & \mathbf{K}_e^{du} \\ \mathbf{K}_e^{ud} & \mathbf{K}_e^{uu} \end{bmatrix} \begin{Bmatrix} \dot{\mathbf{d}} \\ \{\,[[\dot{\mathbf{u}}]]\,\} \end{Bmatrix} = \begin{Bmatrix} \dot{\mathbf{f}}_{int_e} \\ \mathbf{0} \end{Bmatrix} \tag{35}$$

Condensing out $\{\,[[\dot{\mathbf{u}}]]\,\}$ yields:

$$\mathbf{K}_e^{=}\mathbf{K}_e^{dd} - \mathbf{K}_e^{du}\,(\mathbf{K}_e^{uu})^{-1}\,\mathbf{K}_e^{ud} \tag{36}$$

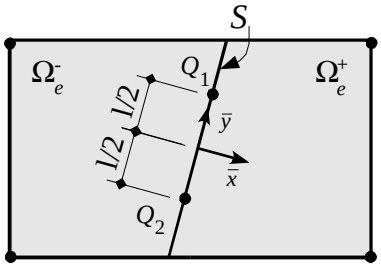

Figure 3: Collocation points on a single interface with non-uniform discontinuity modes.

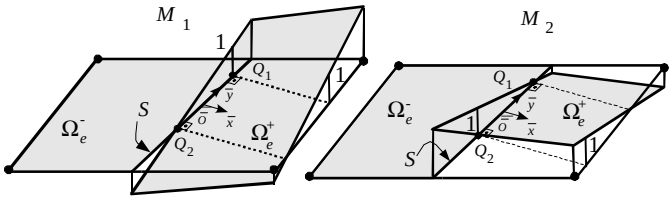

Figure 4: Linear interpolation functions M_1 and M_2.

5 Non-uniform discontinuity modes

Consider an interface discontinuity with two collocation points, Q_1 and Q_2, as shown in Figure 3. Each collocation point introduces a discontinuity jump, $[[\mathbf{u}]]_i$ $(i = 1, 2)$. It is possible to define $\mathbf{P}_1$ and $\mathbf{P}_2$ matrices related to the collocation points, such that:

$$\hat{\mathbf{d}} = [\mathbf{P}]\;\{\,[[\mathbf{u}]]\,\} \tag{37}$$

where

$$[\mathbf{P}] = [\mathbf{P}_1 \quad \mathbf{P}_2] \tag{38}$$

$$\{\,[[\mathbf{u}]]\,\} = \{\,[[\mathbf{u}]]_1 \quad [[\mathbf{u}]]_2\,\}^T \tag{39}$$

Writing the traction continuity Eq.(26) for each collocation point, the resulting formulation is identical to that described for the multiple-discontinuity approach. The $\mathbf{P}_1$ and $\mathbf{P}_2$ matrices can be written as:

$$\mathbf{P}_k = \begin{bmatrix} M_k(\bar{\mathbf{x}}_1) & 0 \\ 0 & M_k(\bar{\mathbf{x}}_1) \\ \vdots & \vdots \\ M_k(\bar{\mathbf{x}}_{n_{en}}) & 0 \\ 0 & M_k(\bar{\mathbf{x}}_{n_{en}}) \end{bmatrix} \quad (k = 1, 2) \tag{40}$$

where $\bar{\mathbf{x}}_i (i = 1, 2, ..., n_{en})$ are the nodal coordinates according to the local system ($\bar{x}$,$\bar{y}$). For instance, the functions $M_k(\bar{\mathbf{x}})$ can be constructed from the linear interpolation functions on S as shown in figure 4.

$$M_1(\bar{\mathbf{x}}) = H(\bar{x})\frac{l/2 + \bar{y}}{l};\; M_2(\bar{\mathbf{x}}) = H(\bar{x})\frac{l/2 - \bar{y}}{l} \tag{41}$$

6 Numerical studies

6.1 Elastoplastic Constitutive Model for the Interface

In the strong discontinuity approach, the non-linear behavior in the interface can be described by a continuum-type constitutive law. In this paper, we use a standard associative elastoplastic constitutive model that can be described by the following set of incremental equations [8]:

$$\dot{\boldsymbol{\sigma}}_h = \mathbf{E}\,(\dot{\boldsymbol{\varepsilon}} - \dot{\boldsymbol{\varepsilon}}^p) \tag{42}$$

$$\dot{\boldsymbol{\varepsilon}}^p = \dot{\lambda}\,\frac{\partial \phi}{\partial \boldsymbol{\sigma}} \tag{43}$$

$$\dot{q} = H(\lambda)\,\dot{\lambda} \tag{44}$$

The loading and unloading situations are distinguished by the Kuhn-Tucker conditions:

$$\phi(\boldsymbol{\sigma}, q) \leq 0, \quad \dot{\lambda} \geq 0, \quad \dot{\lambda}\,\phi(\boldsymbol{\sigma}, q) = 0 \tag{45}$$

where ϕ defines the elastic domain $\phi(\boldsymbol{\sigma}, q) \leq 0$.

To make the constitutive law compatible with strong discontinuity, the plastic multiplier and the inverse of the H modulus must have a distributional character [5], i.e.:

$$\lambda = \delta_S\,\bar{\lambda}; \quad \frac{1}{H(\lambda)} = \delta_S\,\frac{1}{\bar{H}(\bar{\lambda})} \tag{46}$$

The following expressions for the yield surface and softening law are adopted:

$$\phi(\sigma, q) = \sqrt{\frac{2}{3}}\,\|\mathbf{S}\| + p - q \tag{47}$$

$$\bar{H}(\bar{\lambda}) = \frac{\partial q(\bar{\lambda})}{\partial \bar{\lambda}} = -0.95\,\frac{f_t^2}{G_F} e^{-\frac{f_t}{G_F}\bar{\lambda}} \tag{48}$$

where $p = Tr(\boldsymbol{\sigma})/3$ and $\mathbf{S} = \boldsymbol{\sigma} - p\,\mathbf{I}$.

Taking into account the k-regularization Eq.(24) in Eq.(46) yields

$$H(\lambda) = k\left(-0.95\,\frac{f_t^2}{G_F}e^{-\frac{f_t}{G_F}k\lambda}\right) \tag{49}$$

6.2 Basic tests

The numerical study is performed using embedded discontinuity element obtained from the stantard bilinear quadrilateral four-node element [2]. The tests are performed on a square plane stress element, whose geometry and boundary conditions are shown in Figure 5. The material parameters are: E =30 000 Mpa; f_t= 3.0 Mpa; G_F= 0.1 N/mm; ν=0.2.

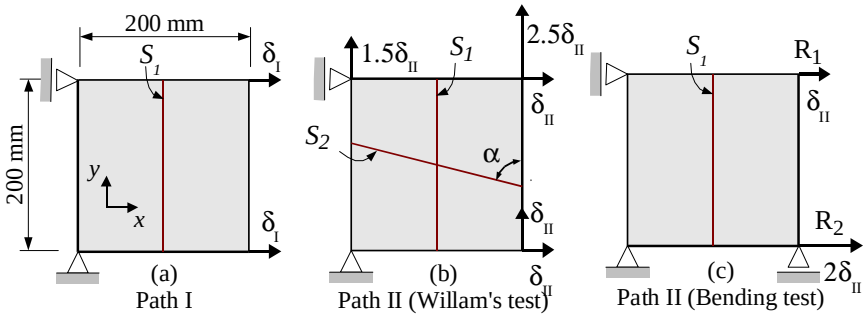

Figure 5: Basic tests.

The initially uncracked specimen is subjected to two consecutive loading paths. In the first one, a monotonically increasing uniaxial tensile stress is applied in the x direction by increasing the horizontal displacement of the right nodes (see Figure 5a). The first loading path ceases when the stress reaches the tensile strength of the material and the first crack line, S_1, forms perpendicular to the first principal stress (see Figure 5a). The second loading path is defined in such a way to characterize two loading scenarios as discussed below.

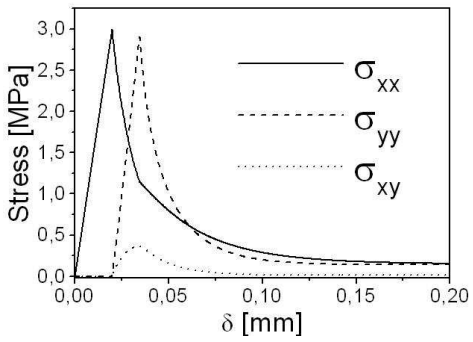

Figure 6: Willam's test: evolution of the stress components.

Willam's Test. To investigate the capacity of the proposed approach to represent multiple embedded discontinuities in the element, the test proposed by Willam et al. [9] has been chosen. In the second

loading path, a strong rotation of the principal directions is imposed by increasing the in-plane total strains ε_{xx}, ε_{yy} and ε_{xy} in the proportion of 1.0: 1.5: 1.0.

The second loading path consists of a monotonically increasing of the nodal displacements according to the scheme shown in Figure 5b. A second crack is allowed to form at an angle perpendicular to the first principal stress if the stress state of the solid portion of the element violates the initiation criterion again.

Figure 6 shows the evolution of the stress components σ_{xx}, σ_{yy} and σ_{xy}. In the second loading path, prior to the second crack initiation, the σ_{xx} stress component decreases while the other components increase due to the progressive rotation of the principal directions of strain. The softening behavior in crack S_1 causes a fast drop of the normal component σ_{xx} and it also prevents a significant increase of the shear component σ_{xy}. Since the evolution of the normal component σ_{yy} is not affected by the crack, the stress state changes gradually from the initial simple tension in the x direction to a single tension in the y direction. When the stress state reaches the initiation criterion again, a second crack forms at an inclination angle of α=77.9 $^\circ$ (see Figure 5b). After the second crack initiation, all stress components decrease leading to a complete stress relaxation of the element.

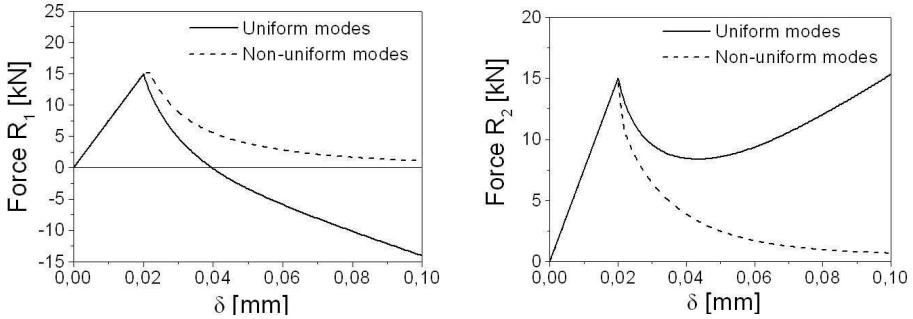

(a) (b)

Figure 7: Bending test: reaction forces versus prescribed displacement.

Bending Test. To assess the performance of the non-uniform discontinuity mode approach, the bending test shown in Figure 5c is also studied. In this case, the second loading path consists of a translation accompanied by a rotation of the right edge of the specimen with respect to the left one.

Figures 7a and 7b show the evolution of the resisting forces R_1 and R_2 at the two right nodes (see Figure 5c).

It can be observed that the approximations using a quadrilateral embedded discontinuity element with a uniform discontinuity mode exhibit a strong stress locking that prevents the relaxation of the resisting forces. The uniform discontinuity mode is incapable to describe a relative rigid-body rotation between the two portions of the element. As a consequence, the imposed rotation of the right edge mobilizes the strain of the elastic solid portion, inducing stress locking.

The resisting forces obtained with the embedded crack element with non-uniform discontinuity modes shows that the stress locking is completely removed by the consideration of non-uniform discontinuity modes.

7 Conclusions

A technique to embed multiple displacement discontinuity interfaces in quadrilateral finite elements has been presented. Non-uniform discontinuity modes can be regarded as a particular case of multiple discontinuities in the element.

The numerical tests show that the technique can successfully model multiple discontinuities and non-uniform discontinuity modes. It is demonstrated that non-uniform modes are crucial to avoid stress locking in quadrilateral elements subjected to bending-type deformation. It is important to notice that this kind of deformation is often found near the crack tip even in structural elements not subjected to bending. The tests also show the good potential of the embedded multiple-discontinuity element to deal with non-proportional load. Future studies concerning the positioning and activation of multiple discontinuities in an element need to be performed to avoid numerical instabilities.

Although the proposed technique has been applied to displacement based bilinear quadrilateral elements, it can be generalized to other types of finite element formulations. This generalization will be addressed in future publication.

Acknowledgements: The financial support from the Brazilian Council for Scientific and Technological Development (CNPq) and the State of São Paulo Research Foundation (FAPESP).

References

[1] E. N. Dvorkin, A. M. Cuitino, and G. Gioia. Finite elements with displacement interpolated embedded localization lines insensitive to mesh size and distortions. *Int. Journ. Num. Meth. Engng.*, 30:541–564, 1990.

[2] T. J. R. Hughes. *The Finite Element Method; linear static and dynamic finite element analysis.* Prenyice-Hall, Englewod Cliffs, N.J., 1987.

[3] M. Jirásek. Comparative study on finite elements with embedded discontinuities. *Comp. Methods Appl. Mech. Engng.*, 188:307–330, 2000.

[4] M. Klisinski, K. Runesson, and S. Sture. Finite element with inner softening band. *ASCE, Journal of Engng. Mechanics*, 3(117):575–587, 1991.

[5] J. Oliver. Modeling strong discontinuities in solid mechanics via strain softening constitutive equations. part 1: Fundamentals. *Int. J. Num. Meth. Eng.*, 21(39):3575–3600, 1996.

[6] J. Oliver. Modeling strong discontinuities in solid mechanics via strain softening constitutive equations. part 2: Numerical simulation. *Int. J. Num. Meth. Eng.*, 21(39):3601–3623, 1996.

[7] J. Oliver, M. Cervera, and O. L. Manzoli. Strong discontinuities and continuum plasticity models: The strong discontinuity approach. *Int. J. of Plasticity*, 3(15):319–351, 1999.

[8] J. C. Simo and T. J. R. Hughes. *Computational Inelasticity.* Springer-Verlag, 1998.

[9] K. Willam, E. Pramono, and S. Sture. Fundamental issues of smeared crack models. In S.P. Shah and S.E. Swartz, editors, *Int. Conf. on Fracture of Concrete and Rock*, pages 192–207, Connecticut, 1987. Society of Engng. Mech.